Breast ultrasound computed tomography using waveform inversion with source encoding

Kun Wang [a], Thomas Matthews [a], Fatima Anis, [a] Cuiping Li[b], Neb Duric[b,c], and Mark A. Anastasio[a]

[a] Department of Biomedical Engineering, Washington University in St. Louis, St. Louis, MO 63130
[b] Delphinus Medical Technologies, Plymouth MI 48170
[c] Karmanos Cancer Inistitute, Wayne State University, Detroit MI 48201

ABSTRACT

Ultrasound computed tomography (USCT) holds great promise for improving the detection and management of breast cancer. Because they are based on the acoustic wave equation, waveform inversion-based reconstruction methods can produce images that possess improved spatial resolution properties over those produced by ray-based methods. However, waveform inversion methods are computationally demanding and have not been applied widely in USCT breast imaging. In this work, source encoding concepts are employed to develop an accelerated USCT reconstruction method that circumvents the large computational burden of conventional waveform inversion methods. This method, referred to as the waveform inversion with source encoding (WISE) method, encodes the measurement data using a random encoding vector and determines an estimate of the speed-of-sound distribution by solving a stochastic optimization problem by use of a stochastic gradient descent algorithm. Computer-simulation studies are conducted to demonstrate the use of the WISE method. Using a single graphics processing unit card, each iteration can be completed within 25 seconds for a 128×128 mm^2 reconstruction region. The results suggest that the WISE method maintains the high spatial resolution of waveform inversion methods while significantly reducing the computational burden.

1. INTRODUCTION

Ultrasound computed tomography (USCT) holds great promise for improving the detection and management of breast cancer. This study will focus on the speed-of-sound (SOS) reconstruction using an existing USCT breast imaging system.[1,2] The USCT imaging system employs a ring-shaped transducer array mounted on the inside wall of a tank. The tank is filled with warm water and placed below a hole on an operating table. In a typical data acquisition, a patient lays in the prone position on the operating table and let her breast pass the hole and suspend in the warm water. One element on the transducer array transmits an acoustic pulse to insonify the breast. The pulse propagates through the breast and water, and the resultant wavefield data are measured by all other elements, completing one data acquisition. By repeating the pulse-transmission and data acquisition procedure sequentially until every transducer element has functioned as the transmitter, one acquires a full data set. The goal of USCT is to reconstruct the SOS distribution of the breast from the acquired data.

To achieve this goal, a wide variety of image reconstruction algorithms have been developed. Most of these algorithms are based on geometrical acoustics, and are commonly referred to as "ray-based" methods.[3–8] While they can be computationally efficient, these methods, in general, result in images with a limited spatial resolution because they neglect high-order acoustic diffraction effects. USCT reconstruction methods based on the acoustic wave equation, also known as full-wave inverse scattering or waveform inversion methods, have also been explored for a variety of applications including medical imaging.[9–12] Because they account for higher-order diffraction effects, waveform inversion methods can produce images that possess higher spatial resolution properties than those produced by ray-based methods.[9,10] However, conventional waveform inversion methods are iterative in nature and require the wave equation to be solved numerically a large number of times at each iteration.

(Send correspondence to:)
Mark Anastasio: E-mail: anastasio@wustl.edu

Consequently, such methods can be extremely computationally burdensome. For special geometries,[12] efficient numerical wave equation solvers have been reported. However, apart from special cases, the large computational burden of waveform inversion methods has hindered their widespread application.

The purpose of this study is to develop an algorithmically-accelerated waveform inversion method for breast SOS reconstruction. Aided by a graphics processing unit (GPU)-accelerated implementation, the developed method will maintain the high spatial resolution of standard waveform inversion methods with a significant reduction in computational time.

2. BACKGROUND: STANDARD WAVEFORM INVERSION

A conventional waveform inversion method seeks the solution of

$$\hat{\mathbf{c}} = \arg\min_{\mathbf{c}} \frac{1}{2} \sum_{m=0}^{M-1} \|\underline{\mathbf{g}_m} - \mathbf{H}^{\mathrm{c}}\mathbf{s}_m\|^2 + \beta\mathcal{R}(\mathbf{c}), \tag{1}$$

where $\mathbf{c}$ is the sought-after object to be reconstructed, i.e, SOS distribution, $\underline{\mathbf{g}_m}$ denotes the measured data vector, $\mathbf{s}_m$ denotes the (known) source vector, $\mathbf{H}^{\mathrm{c}}$ denotes a numerical wave equation solver (NWES) that maps the known source vector to the measured data vector, and $\mathcal{R}(\mathbf{c})$ denotes the penalty term, whose impact is controlled by the regularization parameter β. The superscript in $\mathbf{H}^{\mathrm{c}}$ indicates the dependence of $\mathbf{H}^{\mathrm{c}}$ on $\mathbf{c}$. Note that one USCT measurement involves firing a sequence of acoustic pulses in turn and recording the data corresponding to every pulse. Each pulse-firing and data recording process will be indexed by m for $m = 0, 1, \cdots, M-1$.

A standard gradient descent algorithm, also known as a batch gradient descent algorithm, solves Eqn. (1) iteratively by updating the estimate of $\mathbf{c}$ by taking a small step along the direction opposite the gradient of the cost function. The step size is commonly determined by using a line search method.[13] The conventional waveform inversion method using a batch gradient descent algorithm is described in Alg. 1. In Alg. 1, $\mathbf{J}_m$ denotes

Algorithm 1 Standard waveform inversion using batch gradient descent algorithm.

Input: $\{\underline{\mathbf{g}_m}\}$, $\{\mathbf{s}_m\}$, $\mathbf{c}^{(0)}$
Output: $\hat{\mathbf{c}}$
1: $k \leftarrow 0$ {k is the number of algorithm iteration.}
2: **while** stopping criterion is not satisfied **do**
3: $k \leftarrow k + 1$
4: $\mathbf{J} \leftarrow \sum_{m=0}^{M-1} \mathbf{J}_m + \beta\mathbf{J}^{\mathrm{R}}$ { $\mathbf{J}_m$ and $\mathbf{J}^{\mathrm{R}}$ are the derivative of $\frac{1}{2}\|\underline{\mathbf{g}_m} - \mathbf{H}^{\mathrm{c}}\mathbf{s}_m\|^2$ and $\mathcal{R}(\mathbf{c})$, respectively.}
5: $\mathbf{c}^{(k)} \leftarrow \mathbf{c}^{(k-1)} - \lambda\mathbf{J}$ {Step size λ is determined via a line search}
6: **end while**
7: $\hat{\mathbf{c}} = \mathbf{c}^{(k)}$

the Fréchet dirivative of $\frac{1}{2}\|\underline{\mathbf{g}_m} - \mathbf{H}^{\mathrm{c}}\mathbf{s}_m\|^2$ with respect to $\mathbf{c}$. An adjoint state method has been developed to calculate $\mathbf{J}_m$.[10,14] The method requires the NWES to be run twice, resulting in at least $2M$ NWES runs in every iteration. This makes the batch gradient descent algorithm computationally intensive and greatly limits the application of the waveform inversion method in practice.

3. WAVEFORM INVERSION WITH SOURCE ENCODING

In order to reduce the computational burden, we introduce source encoding concepts that were originally developed in the geophysics literature.[15–17] The proposed waveform inversion with source encoding (WISE) method employs the objective function

$$\hat{\mathbf{c}} = \arg\min_{\mathbf{c}} \mathbf{E}_{\mathbf{w}}\Big\{\frac{1}{2}\|\underline{\mathbf{g}}^{\mathrm{w}} - \mathbf{H}^{\mathrm{c}}\mathbf{s}^{\mathrm{w}}\|^2\Big\} + \beta\mathcal{R}(\mathbf{c}), \tag{2}$$

where $\mathbf{E}_{\mathbf{w}}$ denotes the expectation operator with respect to the random source encoding vector $\mathbf{w} \in \mathbb{R}^M$, and $\underline{\mathbf{g}}^{\mathrm{w}}$ and $\mathbf{s}^{\mathrm{w}}$ denote the $\mathbf{w}$-encoded data and source vectors, defined as

$$\underline{\mathbf{g}}^{\mathrm{w}} = \sum_{m=0}^{M-1} [\mathbf{w}]_m \underline{\mathbf{g}}_m, \quad \text{and} \quad \mathbf{s}^{\mathrm{w}} = \sum_{\mathrm{m}=0}^{\mathrm{M}-1} [\mathbf{w}]_{\mathrm{m}} \mathbf{s}_{\mathrm{m}}, \tag{3}$$

respectively. When $\mathbf{w}$ is zero-mean with an identity covariance matrix, it can be shown that Eqn. (2) is equivalent to Eqn. (1).[16,18,19] Equation (2) can be solved by use of a stochastic gradient descent algorithm,[16,18] summarized in Alg. 2. In Alg. 2, $\mathbf{J}^{\mathrm{w}}$ can be calculated using the same adjoint state method employed in the calculation of

Algorithm 2 WISE using stochastic gradient descent algorithm.

Input: $\{\underline{\mathbf{g}}_m\}$, $\{\mathbf{s}_m\}$, $\mathbf{c}^{(0)}$
Output: $\hat{\mathbf{c}}$
1: $k \leftarrow 0$ {k is the number of algorithm iteration}
2: **while** stopping criterion is not satisfied **do**
3: $k \leftarrow k + 1$
4: Draw elements of $\mathbf{w}$ from independent and identical Rademacher distribution.
5: $\mathbf{J} \leftarrow \mathbf{J}^{\mathrm{w}} + \beta \mathbf{J}^{\mathrm{R}}$ {$\mathbf{J}^{\mathrm{w}}$ is the gradient of $\frac{1}{2}\|\underline{\mathbf{g}}^{\mathrm{w}} - \mathbf{H}^{\mathrm{c}}\mathbf{s}^{\mathrm{w}}\|^2$ for the k-th realization of $\mathbf{w}$.}
6: $\mathbf{c}^{(k)} \leftarrow \mathbf{c}^{(k-1)} - \lambda \mathbf{J}$ {Step size λ is determined via a line search}
7: **end while**
8: $\hat{\mathbf{c}} = \mathbf{c}^{(k)}$

$\mathbf{J}_m$ in Alg. 1. Therefore, the minimum number of NWES runs is reduced from $2M$ to 2, greatly reducing the computational cost at each iteration. Although it, in general, requires more algorithmic iterations to average out the randomness in the realizations of $\mathbf{w}$, the WISE method with the stochastic gradient descent algorithm can greatly reduce the overall number of NWES runs, as demonstrated in the results to follow.

4. DISCRIPTION OF COMPUTER-SIMULATION STUDIES

Computer-simulation studies were conducted to demonstrate the accuracy and efficiency of the proposed WISE method.

4.1 Generation of pressure data

A two-dimensional numerical phantom was employed to represent the SOS distribution in a coronal section of a human breast as shown in Fig. 1-(a). The phantom contains a skin layer and six insertions with SOS values of adipose, parenchyma, cyst, benign tumor and malignant tumor.[20] The object had a diameter of 100 mm and was surrounded by water with SOS 1.5 mm/μs. We employed a ring-shaped transducer array of radius 110 mm to image the breast phantom. The transducer array consists of 256 uniformly-distributed detecting elements, and each element was fired sequentially. The emitted acoustic pulse propagated through the breast, and the resultant wavefield data were recorded by all transducer elements. The wave propagation was calculated using a first-order k-space method-based NWES on a Cartesian grid of spacing 0.25 mm.[21] Sampling at 20 MHz, we calculated 3600 temporal samples for every receiver. The simulated time traces were then undersampled to 10 MHz, resulting in one data acquisition containing 256 time traces with 1800 temporal samples each. Repeating the procedure for all transducers, we generated a noise-free data set containing 256 acquisitions. To the noise-free data set, we added 5% Gaussian white noise to simulate noise-contaminated measurements.

4.2 Image reconstruction

We reconstructed images from the noise-free data set by use of the WISE method using the stochastic gradient descent algorithm described in Alg. 2. A second-order k-space method-based NWES was employed.[22] The NWES was implemented using a grid size 0.5 mm and a sampling rate 10 MHz, both different from the parameters employed to generate the data. For image reconstruction from the noise-free data, no explicit regularization was

employed, i.e., $\beta = 0$ in Eqn. (2). By use of the same NWES, we also implemented the batch gradient descent algorithm described in Alg. 1 for comparison.

From the noisy data set, we reconstructed images by use of the WISE method with a total variation penalty defined as[23,24]

$$\mathcal{R}(\mathbf{c}) = \sum_{j=1}^{N_y-1} \sum_{i=1}^{N_x-1} \sqrt{\epsilon + ([\mathbf{c}]_{jN_x+i} - [\mathbf{c}]_{jN_x+i-1})^2 + ([\mathbf{c}]_{jN_x+i} - [\mathbf{c}]_{(j-1)N_x+i})^2}, \tag{4}$$

where N_x and N_y are the dimensions of the reconstructed image, and $\epsilon = 10^{-12}$ was introduced to avoid dividing by 0 in the gradient calculation. The iteration was terminated when the difference between two consecutive estimates fell below 0.5×10^{-3}. The accuracy of the reconstructed images was quantified by their root-mean-square error (RMSE) from the numerical phantom.

5. NUMERICAL RESULTS

The image reconstructed by use of the WISE method from the noise-free data is shown in Fig. 1-(b), and its profile is plotted in Fig. 2. As confirmed by comparing with the numerical phantom in Fig. 1-(a), the image

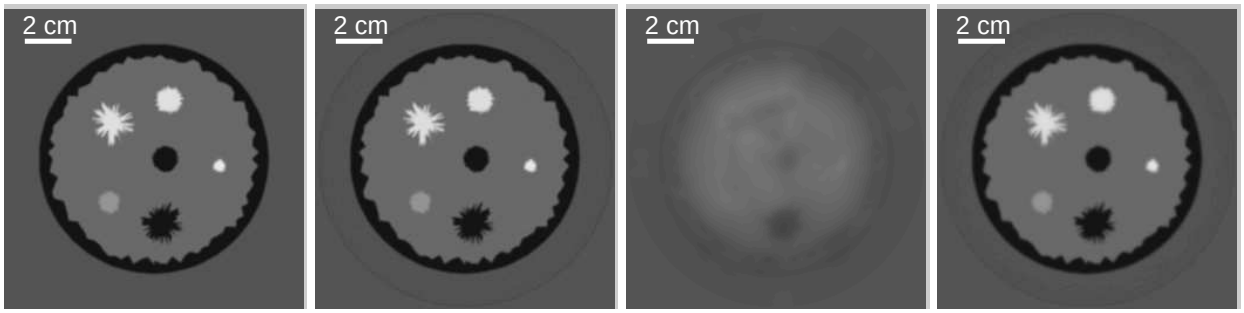

(a) (b) (c) (d)

Figure 1. (a) Numerical breast phantom and images reconstructed by use of (b) the WISE method after the 200-th iteration (1,023 runs of NWES) (c) the conventional waveform inversion method after the 1-st iteration (1,024 runs of the NWES) and (d) the conventional waveform inversion method after the 48-th iteration (61,952 runs of the NWES) from the noise-free data. The grayscale window is $[1.46, 1.58]$ mm/μs.

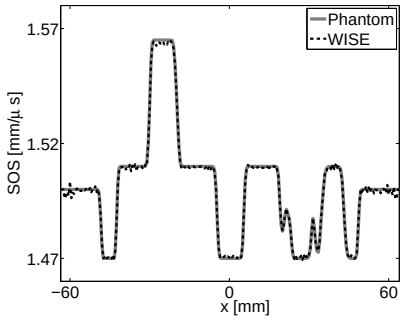

Figure 2. Profile at $y = 7.0$ mm of the image reconstructed by use of the WISE method from the noise-free data.

is highly accurate with a RMSE of 1.10×10^{-3}. The image was obtained after 200 iterations, corresponding to 1023 NWES runs. Approximately half of the NWES runs were due to the line search in Line-6 of Alg. 2. On a platform consisting of an octa-core CPUs with a 3.30 GHz clock speed, 64 gigabytes (GB) of random-accessing memory, and a single NVIDIA Tesla K20 GPU, the computation took 1.3 hours. Within the same computational time, the conventional waveform inversion method only completed 1 iteration (1024 NWES runs). The resultant

image is shown in Fig. 1-(c). This image obviously lacks quantitative accuracy—with a RMSE of 10.94×10^{-3}—as well as qualitative value for identifying features. In order to achieve the same accuracy as the image shown in Fig. 1-(b), the conventional waveform inversion method required 48 iterations or 61952 NWES runs. The computational time was approximately 60 times longer that that required by the WISE method. The resultant image is shown in Fig. 1-(d) with RMSE 1.11×10^{-3}. These results suggest that the WISE method converged to a highly accurate image using less than 2% the time required by a conventional waveform inversion method.

The convergence plots are shown in Fig. 3. As expected, the WISE method, in general, requires more algorithmic iterations to achieve the same RMSE. However, because the computation per each iteration for the WISE method is significantly less than that for the conventional waveform inversion method, the overall computational efficiency remains higher for the WISE method by approximately two-orders of magnitude.

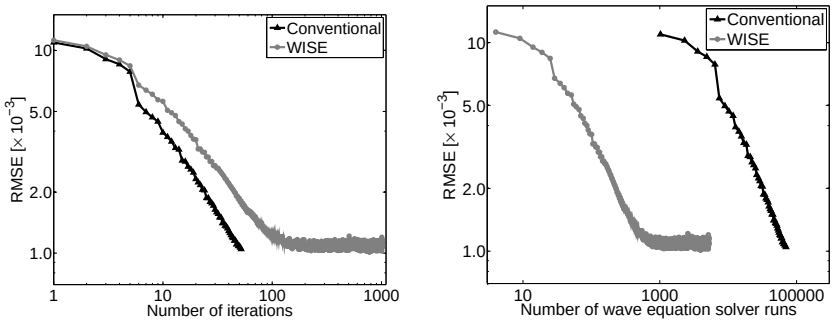

(a) (b)

Figure 3. Plots of the root-mean-square errors (RMSEs) of the images reconstructed from the noise-free data versus (a) the number of iterations and (b) the number of numerical wave equation solver runs.

Figure 4 shows the image reconstructed from the noisy data and its profile. The image was reconstructed after the 1000-th iteration, and the RMSE is 1.33×10^{-3}. These preliminary results suggest that the proposed WISE method is numerically stable.

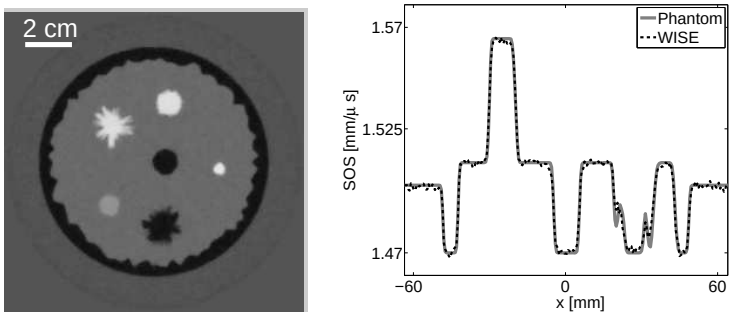

(a) (b)

Figure 4. (a) Image reconstructed by use of the WISE method ($\beta = 5 \times 10^{-4}$) from the noisy data and (b) its profile at $y = 7.0$ mm.

6. SUMMARY

It is known that waveform inversion methods can produce SOS images with higher resolution than do ray-based methods. However, waveform inversion methods are computationally demanding and have not been applied widely in USCT breast imaging. In this work, source encoding concepts are demonstrated in breast USCT experimental studies for the first time. With our current GPU-based implementation, the computation time was reduced from weeks to hours. The results suggest that the method holds value for USCT breast imaging applications in a practical setting.

ACKNOWLEDGMENTS

This work was supported in part by NIH awards EB010049, CA1744601, EB01696301 and DOD Award US ARMY W81XWH-13-1-0233.

REFERENCES

1. Duric, N., Littrup, P., Roy, O., Schmidt, S., Li, C., Bey-Knight, L., and Chen, X., "Breast imaging with ultrasound tomography: Initial results with softvue," in [*Ultrasonics Symposium (IUS), 2013 IEEE International*], 382–385 (July 2013).
2. Duric, N., Littrup, P., Li, C., Roy, O., Schmidt, S., Cheng, X., Seamans, J., Wallen, A., and Bey-Knight, L., "Breast imaging with softvue: initial clinical evaluation," *Proc. SPIE* **9040**, 90400V–90400V–8 (2014).
3. Kak, A. C. and Slaney, M., [*Principles of Computerized Tomographic Imaging*], IEEE Press (1988).
4. Hesford, A. J. and Chew, W. C., "Fast inverse scattering solutions using the distorted born iterative method and the multilevel fast multipole algorithm," *J. Acoust. Soc. Am.* **128**(2) (2010).
5. Lavarello, R. J. and Oelze, M. L., "Density imaging using a multiple-frequency DBIM approach," *IEEE. T. Ultrason. Ferr.* **57**, 2471–2479 (November 2010).
6. Hormati, A., Jovanovi, I., Roy, O., and Vetterli, M., "Robust ultrasound travel-time tomography using the bent ray model," in [*Proc. SPIE*], **7629**, 76290I–76290I–12 (2010).
7. Li, C., Huang, L., Duric, N., Zhang, H., and Rowe, C., "An improved automatic time-of-flight picker for medical ultrasound tomography," *Ultrasonics* **49**(1), 61–72 (2009).
8. Li, C., Duric, N., and Huang, L., "Breast ultrasound tomography with total-variation regularization," in [*Proc. SPIE*], **7265**, 726506–726506–8 (2009).
9. Pratt, R. G., Huang, L., Duric, N., and Littrup, P., "Sound-speed and attenuation imaging of breast tissue using waveform tomography of transmission ultrasound data," in [*Proc. SPIE*], **6510**, 65104S–65104S–12 (2007).
10. Roy, O., Jovanović, I., Hormati, A., Parhizkar, R., and Vetterli, M., "Sound speed estimation using wave-based ultrasound tomography: theory and GPU implementation," in [*SPIE Medical Imaging*], 76290J–76290J, International Society for Optics and Photonics (2010).
11. Zhang, Z., Huang, L., and Lin, Y., "Efficient implementation of ultrasound waveform tomography using source encoding," in [*SPIE Medical Imaging*], 832003–832003, International Society for Optics and Photonics (2012).
12. Wiskin, J., Borup, D. T., Johnson, S. A., and Berggren, M., "Non-linear inverse scattering: High resolution quantitative breast tissue tomography," *J. Acoust. Soc. Am.* **131**(5), 3802–3813 (2012).
13. Nash, S. and Sofer, A., [*Linear and Nonlinear Programming*], New York: McGraw-Hill (1996).
14. Norton, S. J., "Iterative inverse scattering algorithms: Methods of computing Fréchet derivatives," *J. Acoust. Soc. Am.* **106**(5), 2653–2660 (1999).
15. Krebs, J. R., Anderson, J. E., Hinkley, D., Neelamani, R., Lee, S., Baumstein, A., and Lacasse, M.-D., "Fast full-wavefield seismic inversion using encoded sources," *Geophysics* **74**(6), WCC177–WCC188 (2009).
16. Haber, E., Chung, M., and Herrmann, F., "An effective method for parameter estimation with PDE constraints with multiple right-hand sides," *SIAM J. Optimiz.* **22**(3), 739–757 (2012).
17. Moghaddam, P. P., Keers, H., Herrmann, F. J., and Mulder, W. A., "A new optimization approach for source-encoding full-waveform inversion," *Geophysics* **78**(3), R125–R132 (2013).
18. Haber, E. and Chung, M., "Simultaneous source for non-uniform data variance and missing data," *arXiv preprint arXiv:1404.5254* (2014).
19. Roosta-Khorasani, F., van den Doel, K., and Ascher, U. M., "Data completion and stochastic algorithms for PDE inversion problems with many measurements," *CoRR* **abs/1312.0707** (2013).
20. Szabo, T. L., [*Diagnostic ultrasound imaging: inside out*], Academic Press (2004).
21. Tabei, M., Mast, T. D., and Waag, R. C., "A k-space method for coupled first-order acoustic propagation equations," *J. Acoust. Soc. Am.* **111**(1), 53–63 (2002).

22. Mast, T., Souriau, L., Liu, D.-L., Tabei, M., Nachman, A., and Waag, R., "A k-space method for large-scale models of wave propagation in tissue," *Ultrasonics, Ferroelectrics and Frequency Control, IEEE Transactions on* **48**, 341–354 (March 2001).
23. Sidky, E. Y. and Pan, X., "Image reconstruction in circular cone-beam computed tomography by constrained, total-variation minimization," *Phys. Med. Biol.* **53**(17), 4777 (2008). http://stacks.iop.org/0031-9155/53/i=17/a=021.
24. Wang, K., Sidky, E. Y., Anastasio, M. A., Oraevsky, A. A., and Pan, X., "Limited data image reconstruction in optoacoustic tomography by constrained total variation minimization," *Photons Plus Ultrasound: Imaging and Sensing 2011* **7899**(1), 78993U, SPIE (2011).